Carbohydrate Polymers 117 (2015) 355–363

Contents lists available at ScienceDirect

Carbohydrate Polymers

journal homepage: www.elsevier.com/locate/carbpol

Monitoring of cellulose depolymerization in 1-ethyl-3-methylimidazolium acetate by shear and elongational rheology

Anne Michud [a], Michael Hummel [a], Simon Haward [b], Herbert Sixta [a,*]

[a] Department of Forest Products Technology, Aalto University, School of Chemical Technology, Aalto, PO Box 16300, 00076, Espoo, Finland
[b] Departamento de Engenharia Quımica, CEFT, Faculdade de Engenharia da Universidade do Porto, Rua dr Roberto Frias s/n, 4200-465 Porto, Portugal

ARTICLE INFO

Article history:
Received 14 August 2014
Received in revised form 9 September 2014
Accepted 21 September 2014
Available online 7 October 2014

Keywords:
Cellulose
Cellulose degradation
Ionic liquid
Rheological characterization

ABSTRACT

The thermal stability of cellulose in the ionic liquid (IL) 1-ethyl-3-methylimidazolium acetate, [emim]OAc was investigated. For this purpose, *Eucalyptus urugrandis* prehydrolysis kraft pulp was first dissolved in [emim]OAc by means of a vertical kneader and then stored at three different temperatures to study the time-depended behavior of the cellulose-[emim]OAc system. Cellulose depolymerization was assessed by characterizing the precipitated cellulose and the rheological behavior of the cellulose-[emim]OAc solutions. The results show decreases in the weight average molecular mass and in the shear viscosity at temperatures exceeding 60 °C, which can be related to progressing degradation of cellulose in the IL upon storage at elevated temperature. The changes in behavior of the solutions under extensional stresses also attest the gradual depolymerization of cellulose. The degradation has been analyzed using appropriate kinetic models. Propyl gallate appeared to be an efficient stabilizer of the cellulose-[emim]OAc system during the dissolution step even though the mechanism has not been fully understood yet.

1. Introduction

Over the last decades, the demand for consumption goods has significantly increased due to the world population growth and a rise in per-capita consumption, especially in developing countries. Concomitantly, growing concerns regarding the use of depleting crude oil feedstock as well as an increasing awareness towards sustainable resource management has raised the interest in the use of biodegradable and organic renewables. Cellulose being the most abundant natural polymer on earth offers opportunities as raw material for many applications.

The market for sustainable cellulose products such as films, foils, composite or man-made cellulosic (MMC) fibers, is expanding worldwide. In 2012, the total fiber consumption was 83.5 million tons (The Fiber Year, 2013) of which 33% were cellulosic fibers (cotton, Viscose/Rayon, Modal and Tencel® fibers). In 2012, cotton represented 82% of the total consumption of cellulosic fibers. However, owing to limited cotton production and thus increasing cotton costs, the cotton output decreased by 5.4% over the period 2011–2012. Moreover, the large amount of water required for its production and the extensive use of artificial fertilizers and pesticides can make cotton an unsustainable cellulosic fiber raw material (The Fiber Year, 2013). A study for the period 2010–2030 predicts an annual fiber production of 133.5 million tons in 2030 with an estimated share of 33 to 37% of cellulosic fibers, thus raising the demand of cellulosic fibers to 44–49 million tons in 2030. Assuming a maximum cotton production of 26 million tons, 18 to 23 million tons of MMC fibers will be needed to fill the so-called cellulose gap (Eichinger, 2012).

Nowadays, the market of man-made cellulosic fibers, cellulosic films and composites is still dominated by the viscose process that uses and forms highly toxic chemicals and gasses and, consequently, may pose a threat to the environment. The more environmentally acceptable lyocell process, commercialized in the early 1990s, using the non-derivatizing solvent *N*-methylmorpholine *N*-oxide (NMMO) has been so far the only viable alternative to the viscose process (Fink, Weigel, Purz, & Ganster, 2001). However, the thermal instability of NMMO demands important investments in safety technology to avoid thermal run-away reactions and cellulose degradation. Moreover, films manufactured with the viscose process show inferior barrier and mechanical properties compared to synthetic films. Therefore, new industrial technologies for the processing of cellulose

* Corresponding author. Tel.: +358 50 384 1764; fax: +358 9 470 24259.
E-mail addresses: anne.michud@aalto.fi (A. Michud), michael.hummel@aalto.fi (M. Hummel), shaward@fe.up.pt (S. Haward), herbert.sixta@aalto.fi (H. Sixta).

http://dx.doi.org/10.1016/j.carbpol.2014.09.075
0144-8617/

in direct solvents are desired to manufacture cellulosic material with outstanding properties and to make their production cost- and eco-efficient (Hermanutz, Gähr, Uerdingen, Meister, & Kosan, 2008; Perepelkin, 2007). Ionic liquids that have been presented as a novel class of direct solvents for cellulose have been thoroughly investigated during the last few years. They appear to be a promising alternative to NMMO and offer new possibilities for cellulose processing (Cao et al., 2009; Feng & Chen, 2008; Kosan, Michels, & Meister, 2008; Swatloski, Spear, Holbrey, & Rogers, 2002). Their low melting point, low vapor pressure, thermal stability and their ability to dissolve cellulose of high DP make ILs advantageous for industrial processes (Pinkert, Marsh, Pang, & Staiger, 2010). Furthermore, the possibility of preparing mixtures of cellulose with different substrates or activation of cellulose in ILs makes them attractive especially for the production of biocomposite (Simmons et al., 2011; Stefanescu, Daly, & Negulescu, 2012; Wu, Wang, Li, Li, & Wang, 2009).

The stability of dissolved cellulose in ionic liquids upon thermal impact is of special importance for the processing conditions of shaped cellulosic products such as films, composites or fibers. The high temperature used during the different preparation steps, from the dissolution until the regeneration of cellulose, may cause cellulose depolymerization (Haward, Sharma, Butts, McKinley, & Rahatekar, 2012; Wendler, Kosan, Krieg, & Meister, 2009). The intrinsic viscosity measurement is a fast and convenient method to estimate the average DP of cellulose and thus the extent of degradation. However, the determination of DP provides only some information on the viscosity-average molar mass and no element regarding the molar mass distribution (MMD). A polymer cannot be fully characterized by a single molecular mass value; it is well defined by a molar mass distribution which is one of the key factors affecting the rheology of a visco-elastic cellulose–IL solution and, thus, its processability during coagulation (Collier, Watson, Collier, & Petrovan, 2009; Dupont & Mortha, 2004). The assessment of cellulose degradation through the determination of the MMD requires the regeneration of the dissolved cellulose in ILs. This method is consequently time-consuming and necessitates being performed offline between the dissolution and shaping regeneration steps. Unlike the traditional methods to quantify the intrinsic properties of dissolved cellulose, rheological measurements offer the possibility of on-line monitoring the extent of cellulose depolymerization. Visco-elastic properties of cellulose–IL solution are dependent of the DP and MMD of dissolved cellulose. Thus, the change of the complex viscosity or the extensional viscosity of cellulose–IL can be used to determine whether the cellulose degrades during the process (Lu, Cheng, Song, & Liang, 2012). Moreover, shear and extensional deformations play a major role in cellulose processing operations which involve rapid change of shape such as fiber spinning or film blowing. The assessment of the rheological properties of cellulose–IL solution is, hence, a prerequisite for successful cellulose processing (Sammons, Collier, Rials, & Petrovan, 2008a,b; Sammons et al., 2008a,b). Rheological characterization of cellulose–IL solutions is thus an important method for monitoring cellulose degradation and fundamental for the subsequent processing of polymer solutions.

In this study, we use *Eucalyptus urugrandis* prehydrolysis kraft pulp dissolved in 1-ethyl-3-methylimidazolium acetate to demonstrate how cellulose depolymerization upon storage in ILs at high temperatures can be monitored by shear and elongation rheology. Cellulose degradation is first assessed by traditional methods through the determination of the intrinsic viscosity and the MMD of the regenerated cellulose. The kinetics of cellulose depolymerization is calculated using two model types. In the second part, the shear and elongational properties of the cellulose–IL solution are evaluated in order to show how the intrinsic properties of the regenerated cellulose and the rheological properties of the cellulose–IL solution can be linked and, hence, how the rheological properties of cellulose–IL solution can be directly used to estimate the extent of cellulose depolymerization.

2. Experimental

2.1. Materials and methods

E. urugrandis prehydrolysis kraft pulp (PHKeuca DP = 1026 calculated from the intrinsic viscosity, M_n = 79.8 kDa, M_w = 268.6 kDa, polydispersity 3.4, Bahia Speciality Cellulose, Brazil) was used as cellulosic solute. This pulp grade is typically used for the production of man-made cellulose fibers. It contains 2.5% of hemicellulose and has a kappa number of 0.69. The pulp was delivered in sheet form and cut to a powder by means of a Willey mill. 1-Ethyl-3-methylimidazolium acetate (purity ≥95%) was purchased from BASF (Germany) and used without any further purification. A water content of 0.13% was determined via Karl-Fischer titration. *N*,*N*-dimethylacetamide (DMAc) and lithium chloride (LiCl; analytical grade), used for the molar mass distribution characterization, and propyl gallate (PG, analytical grade) used as a stabilizer during the dissolution of cellulose in [emim]OAc were purchased from Sigma-Aldrich.

2.1.1. Preparation of cellulose-[emim]OAc solution

The dissolution of cellulose in [emim]OAc was carried out in a vertical kneader system following a protocol earlier suggested for the preparation of [emim]OAc-based spin dopes (Kosan et al., 2008). Temperature, pressure, torque moment and revolution per minute (rpm) versus reaction time were controlled online (Hauru et al., 2013). The PHKeuca pulp was first swollen in water to increase the accessibility of the hydroxyl groups. [emim]OAc was then added to the swollen pulp and the ternary mixture (cellulose–IL–water) was finally transferred to the vertical kneader. PG (2 wt% on dry cellulose) was added to the suspension when preparing a stabilized cellulose solution. The pulp was dissolved at 95 °C and 48 rpm. Excessive water was removed at reduced pressure (down to 55 mbar). The dissolution phase was indicated by a significant increase of the torque moment until the mixture forms a gel-like structure (Kosan et al., 2008). Upon further progress of the dissolution, the gel is turned into a real solution resulting in a small decrease of the torque after which the solution was stirred for another hour to ensure complete dissolution. Any undissolved particles or impurities were removed afterward by means of a hydraulic pressure filtration unit (metal fleece filter of ca. 5 μm absolute pore size). A dope of 10 wt% of cellulose in 1-ethyl-3-methylimidazolium acetate was prepared, then divided into three portions for the degradation series, and sealed tightly.

2.1.2. Degradation of cellulose solution

The cellulose-[emim]OAc solutions were stored for 24 h in an oven at 60, 90 and 110 °C. Samples were taken after 1, 2, 4, 8 and 24 h for the three temperatures. The samples were sealed again and stored in solution state from which the cellulose was regenerated for further characterization. The PG-stabilized cellulose solution was degraded at 110 °C for 1, 2, 4, 8 and 24 h.

2.1.3. Coagulation of cellulose

The coagulation of the dissolved cellulose in [emim]OAc was performed by adding water as an anti-solvent. A high shear mixer (IKA Ultra Turrax) was used to disintegrate the coagulated cellulosic film into flake-like cellulose. The resulting cellulose was filtrated and washed three times to eliminate any remaining ionic liquid. The coagulated flakes were then dried at room temperature for two days. Oven-dried cellulose samples showed hornification

phenomena and were difficult to re-dissolve for intrinsic viscosity and GPC measurements.

2.2. Analyses

2.2.1. Characterization of coagulated cellulose

Intrinsic viscosity, $[\eta]$, of the coagulated cellulose was determined in cupriethylenediamine (CED) according to SCAN-CM 15:99. The degree of polymerization (DP_v) was then calculated according to the following equations:

$$DP_v = \left(\frac{[\eta]}{2.28}\right)^{1/0.76} \quad \text{for} \quad \eta > 400\,\text{ml/g} \tag{1}$$

$$DP_v = \frac{[\eta]}{0.42} \quad \text{for} \quad \eta < 400\,\text{ml/g} \tag{2}$$

Molar mass distribution was determined by a GPC-system consisting of a pre-column (PLgel Mixed-A, 7.5 × 50 mm), four analytical columns (4 × PLgel Mixed-A, 7.5 × 300 mm) and a RI-detector (Shodex RI-101). After a sequence of activation in water, acetone and DMAc, cellulose was dissolved in 90 g/l LiCl/DMAc at room temperature under a constant slow speed magnetic stirring. After dissolution, the sample was diluted in pure DMAc to reach a concentration of 1 mg/ml in 9 g/l LiCl/DMAc. The samples were then filtered with 0.2 μm syringe filters and a volume of 100 μl was separated at 25 °C at a flow rate of 0.750 ml/min with 9 g/l LiCl/DMAc as eluent. Calibration was done using pullulan standards with molecular weights ranging from 343 Da to 708,000 Da. Molar mass distributions of cellulose obtained by performing GPC/RI by direct-standard-calibration were then corrected using an algorithm calculating cellulose-equivalent molar masses of pullulan standards ($MM_{cellulose} = q \times MM^{P}_{pullulan}$) as suggested by Berggren, Berthold, Sjöholm, and Lindström (2003) and Borrega, Tolonen, Bardot, Testova, and Sixta (2013). The coefficients $q = 12.19$ and $p = 0.78$ were found by a least-square method, using the data published in their report.

2.2.2. Kinetics of cellulose degradation

Degradation of cellulose is mainly due to the cleavage of the β-glucosidic bonds along the cellulose chains. The kinetic of cellulose degradation in [emim]OAc was analyzed using two models. They describe the extent of cellulose degradation in terms of the number of scissions of the β-glucosidic bonds per cellulose chain and thus use the evolution of the degree of polymerization in their determination. The first model, described by Eq. (3), corresponds to the difference between two reciprocal degrees of polymerization. However, the experimental uncertainty of the DP values is amplified in this method. Calvini and Gorassini (2006) suggested that a ratio between the values of DP should be introduced into the rate equation of cellulose degradation that is given by Eq. (4) (Calvini, Gorassini, & Merlani, 2008; Ding & Wang, 2008). The notion of levelling-off degree of polymerization (LODP) was introduced by Calvini (2005) into the kinetic model of cellulose degradation through the initial number of cellulose bonds available for the degradation n° as can been seen in Eqs. (3) and (4). It has to be noted that herein the LODP is a free parameter in the non-linear least square fit and, thus, representing the calculated limiting DP value only.

$$\text{Model 1} \quad S = \left(\frac{1}{DP} - \frac{1}{DP_0}\right) = n^\circ \times \left(1 - e^{-kt}\right) = \left(\frac{1}{LODP} - \frac{1}{DP_0}\right) \times \left(1 - e^{-kt}\right) \tag{3}$$

$$\text{Model 2} \quad S = \left(\frac{DP_0}{DP - 1}\right) = n^\circ \times \left(1 - e^{-kt}\right) = \left(\frac{DP_0}{LODP - 1}\right) \times \left(1 - e^{-kt}\right) \tag{4}$$

2.2.3. Rheological characterization of cellulose solutions

Surface tension and density of the dopes, needed for the extensional characterization, were determined via KSV CAM contact angle and surface tension meter modified with a dry cell and an Anton Paar DMA515 density meter, respectively. The cellulose–IL solutions showed a surface tension of 35 mN/m and a density of 1.111 g/cm^3.

Oscillatory shear rheology of the different samples was measured on an Anton Paar MCR 300 with a plate and plate geometry. Time stability tests showed no significant moisture uptake from the laboratory atmosphere at the plate edges within the required testing time. Thus, it was not necessary to seal the edges with paraffin oil as previously suggested by others (Gericke, Schlufter, Liebert, Heinze, & Budtova, 2009; Sammons et al., 2008a,b). Dynamic strain sweep tests were first performed to define the viscoelastic domain. A strain of 1% was chosen for the subsequent frequency sweep tests which were carried out over an angular velocity range, ω, of 0.01–100 s^{-1} at 60 °C. Complex viscosity, η^*, as well as dynamic moduli, G' and G'' representing the storage modulus and loss modulus respectively, were recorded. As suggested by Sammons et al., complex viscosity data were fitted to the three-parameter Cross viscosity model, given by Eq. (5), to determine the zero shear viscosity, η_0 (Sammons et al., 2008a,b). The Cox–Merz rule is here assumed to be valid (Lu et al., 2012).

$$\eta = \frac{\eta_0}{\left(1 + (\lambda\dot{\gamma})^{1-n}\right)} \tag{5}$$

where λ is a time constant and n is the power-law exponent.

Extensional rheological analyses were conducted on a thermo fisher capillary break-up extensional rheometer (CaBER) at 60 °C. In this breakup device, the solution is first loaded between two plates. Prior to the actual measurement, the upper plate is rapidly moved up and then held at a fixed vertical displacement. A liquid thread is thus formed and the evolution of the mid-filament diameter is monitored as a function of time by a laser micrometer until its final breakup (Anna & McKinley, 2001; Stelter, Brenn, Yarin, Singh, & Durst, 2000). Plates of 6 mm were used and the step-stretch defined by an initial and final aspect ratio of 0.66 and 3, respectively (initial and final separation of 2 and 9 mm, respectively). After sample loading, a defined equilibration time of 2 min was waited before the start of the measurement in order to let the cellulose chains fully relax. Possible moisture up-take during the measurement was prevented by purging a dry air flow of 1.5 ml/min through the measurement cell. The effective sample temperature was determined by a Testo 845 contactless IR thermometer.

A set of forces balancing each other divide the self-thinning of the thread into four regimes. In the first regime (I), the fluid cylinder is exposed to gravitational forces which are opposing the capillary forces and which distort the assumed axial symmetry around the mid-plane of the filament thread. A lower boundary to this regime can be defined by the Bond number Bo, given by Eq. (6), using the density ρ and the surface tension γ of the solution, the gravitational constant g, and the local filament radius $R(t)$. For radii resulting in $B_0 < 0.2$, gravitational effects can be neglected (Clasen, 2010). In our case, data deriving from a diameter higher than 1.60 mm should be disregarded.

$$B_0 = \frac{\left(\rho g R^2\right)}{\gamma} \tag{6}$$

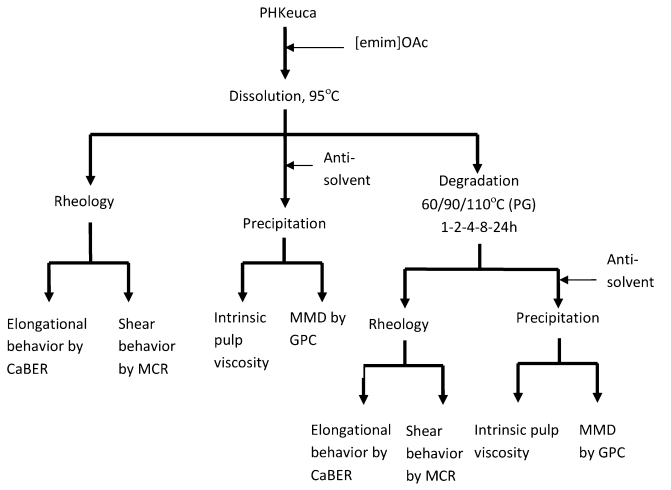

Fig. 1. Flow chart showing experimental steps and performed analyses.

In the second regime (II), the polymer solution exhibits Newtonian-like behavior, the filament diameter decreases slowly and linearly with time. The capillary forces γ/R that drive the filament thinning are balanced by the material's viscous tensile stresses $\eta_E\dot{\varepsilon}$, apparent extensional viscosity and extension rate respectively, that predominate the elastic tensile stresses. The filament diameter being still large, the extension rate $\dot{\varepsilon}$ is low and the cellulose chains are not stretched yet. In the third regime (III), the filament thinning is still controlled by a visco-capillary balance of the capillary pressure and the viscous stresses present in the filament. However, the polymer solution shows an extensional thinning due to the higher surface pressure and thus extension rate. An increase in the disentanglement and orientation of the polymer chains is noticed in this regime. The onset of the elasto-capillary balance is observed in the fourth regime (IV) with the elastic stresses prevailing the viscous stresses within the filament and balancing the action of the capillary pressure. The diameter decay at this stage is described by an exponential function. This regime only takes place at very small diameters close to breakup (Anna & McKinley, 2001; Clasen, 2010; Stelter, Brenn, Yarin, Singh, & Durst, 2002).

From the decay of the filament diameter (in mm), the breakup time (in s), the apparent extensional viscosity (in Pa s) and the extension rate (in s^{-1}) can be calculated by the following equations:

$$\eta_E = \frac{\gamma}{2\left(dR/dt\right)} \tag{7}$$

$$\dot{\varepsilon} = -\frac{2dR}{(Rdt)} \tag{8}$$

2.2.4. Experimental steps and analysis of the investigation

Fig. 1.

3. Results and discussion

3.1. Characterization of regenerated cellulose

3.1.1. Degree of polymerization

The extent of cellulose depolymerization was first assessed by characterizing the degree of polymerization via the intrinsic viscosity, [η], and the molar mass distribution (MMD) of the precipitated cellulose of the different samples.

Table 1 summarizes the analytical data of the regenerated cellulose. The dissolution step was carried out using prehydrolysis kraft pulp with an intrinsic viscosity [η] of 443 ml/g corresponding to a DP_v of 1026. A significant DP-degradation of 25.2% was detected

Table 1
Intrinsic characteristic of regenerated cellulose from cellulose-[emim]OAc dopes.

Original pulp	DP_v	DP-degradation (%)				M_n (kDa)				M_w (kDa)				M_z (kDa)				PDI			
	1026	-				79.8				268.6				644.5				3.4			
Storage temperature	110 °C	110 °C				110 °C				110 °C				110 °C				110 °C			
	60 °C	90 °C	–	PG	60 °C	90 °C	–	PG	60 °C	90 °C	–	PG	60 °C	90 °C	–	PG	60 °C	90 °C	–	PG	60 °C	90 °C	–	PG
Storage time 0 h[a]		767[c]			993[c]																			
1 h[b]	775	764	755	955	0.0[d]	0.4	1.6	3.8	80.3	90.7	82.3	116.2	178.4	190.1	166.0	240.1	337.2	348.4	314.0	416.8	2.3	2.1	2.0	2.1
2 h	764	736	730	914	0.0	4.0	4.8	7.9	79.4	80.8	68.5	87.5	174.1	185.5	145.9	230.6	311.0	362.4	277.0	433.6	2.2	2.3	2.1	2.7
4 h	788	732	701	879	0.0	4.7	8.6	11.5	77.7	79.3	78.2	91.6	184.3	182.9	159.4	227.0	377.1	350.6	288.5	430.0	2.4	2.3	2.1	2.5
8 h	769	713	700	849	0.0	7.0	8.7	14.5	97.9	77.1	66.5	120.6	184.6	178.7	145.3	227.0	317.9	347.2	280.4	370.5	1.9	2.3	2.2	1.9
24 h	–	700	676	828	–	8.7	11.9	16.6	–	60.9	74.4	95.0	–	166.7	148.6	224.4	–	342.5	270.1	399.1	–	2.8	2.0	2.4

[a] Characterization of precipitated cellulose after dissolution.
[b] Characterization of precipitated cellulose after a storage time of 1 h in the oven.
[c] DP_v of precipitated cellulose after the dissolution step.
[d] DP_v-degradation of cellulose taking the DP_v of cellulose after the dissolution step as reference.

Table 2
Evolution of cellulose chain fraction upon time at 110 °C.

	DP < 50 (%)	DP < 100 (%)	DP > 2000 (%)
Original pulp	1.1	3.2	25.7
0 h	0.0	2.3	13.5
1 h	0.0	1.3	11.5
4 h	0.2	1.6	10.7
24 h	0.1	1.7	9.2

after the dissolution step. This marked reduction can be explained by the high temperature (95 °C) and the shear forces needed for a fast dissolution. The extent of degradation is reduced to about 10% when dissolving the same pulp at a temperature of 85 °C. The DP_v values of the precipitated cellulose from the cellulose–IL solutions that have been kept at 60, 90 and 110 °C for specified times as well as the relative DP-degradation in percent are given in Table 1. The DP_v values show stability of the cellulose-[emim]OAc system at a temperature of 60 °C; no polymer chain scissions are taking place. However, cellulose degradation occurs at 90 and 110 °C. Cellulose depolymerization is naturally more pronounced at 110 °C than at 90 °C resulting in a final DP_v-reduction of 11.9% and 8.7% after 24 h of storage, respectively. The rate of cellulose depolymerization decreases with storage time, regardless of the storage temperature.

In this study, [emim]OAc of purity ≥95% was purchased from BASF and was used without any further purification. Some impurities, such as tertiary amines, methyl- and ethylimidazole, and metal cations, are generally formed during the synthesis process or heating of ILs and can be involved in further side-reactions or may act as catalysts. Another major impurities to consider is water which significantly influences the dissolution process and participates in the thermal decomposition of [emim]OAc (Liebert & Heinze, 2008; Wendler, Todi, & Meister, 2012).

Propyl gallate, standard stabilizer in the lyocell process, is a phenolic antioxidant acting as a radical scavenger. Its role is to form radicals, which interrupt the reaction chain and yield stable products in subsequent reactions. PG reacts with radical species present in solution and forms the relatively stable phenoxyl radicals which recombine to ellagic acid via carbon-carbon coupling. Ellagic acid being a phenolic antioxidant itself is converted by four radical equivalents into the deeply colored conjugated compound bis(*ortho*-quinone) (Rosenau et al., 2002). A discoloration of the cellulose–IL solution was observed few seconds after adding PG to [emim]OAc demonstrating the action of propyl gallate as a radical trap. Impurities such as metal ions can also be complexed by the stabilizer before the formation of metal-induced radicals. As seen in Table 1, the use of PG as stabilizer influences significantly the cellulose depolymerization during the dissolution of cellulose in [emim]OAc. The addition of 2% PG (on dry cellulose) decreases the DP_v-degradation from 25.2% to 3.2%.

3.1.2. Molar mass distribution

In order to gain a better understanding of the depolymerization, the molar mass distribution and the polydispersity index (PDI) of the regenerated cellulose were determined. Table 1 summarizes the different molecular weight averages (M_n, M_w, and M_z) and PDI of the original and the regenerated cellulose after dissolution and storage at elevated temperature. The evolution of the cellulose chain fractions of the different molecular weight at 110 °C is represented in Table 2. The decrease of M_w is in line with the decrease of the DP_v, indicating the gradual degradation of cellulose over time. Furthermore, a strong temperature dependency of the degradation is observed. In Fig. 2, the shift of the MMD to lower molecular weights illustrates the significant degradation of cellulose occurring during the dissolution of cellulose and the first hour of storage at 110 °C. Lower shifts are noticed for storage times

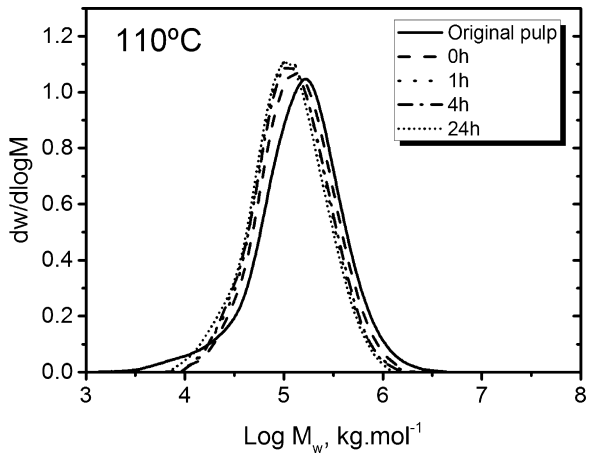

Fig. 2. Molar mass distribution of the original pulp, precipitated cellulose after dissolution and after storage at 110 °C.

higher than 1 h. The degradation occurring at 110 °C during the dissolution step is also indicated in Table 2 by the significant decrease of the different molecular weight fractions of cellulose. The low molecular weight cellulose chains are completely missing in the coagulated samples (see Fig. 2). This lost fraction might correspond to the hemicellulose present in the original pulp which is degraded to oligosaccharides during the dissolution step. The solvation of hemicellulose is favored over cellulose in IL-water mixture (Roselli, Hummel, Monshizadesh, Maloney, & Sixta, 2014) and thus the short chain xylo-oligosacharrides are difficult to recover upon addition of water. Moreover, Table 2 shows the reduction of high molecular weight cellulose chains as the thermal treatment time increases. The slight decreases of the M_w of stabilized cellulose, indicated in Table 1, show the efficiency of PG during the dissolution. The steady PDI values indicate a homogeneous degradation along cellulose chains.

3.1.3. Kinetics of cellulose degradation

The kinetics of cellulose degradation was investigated by calculating the number of scission per cellulose chain using two different models, described by Eqs. (3) and (4). Fig. 3 depicts the average number of scission per chain unit during the degradation process over time at 60, 90 and 110 °C using model 2. Fig. 3a shows the number of chain scission calculated by using the DP_v of the original pulp as DP_0. The severe degradation of cellulose occurring during the dissolution process was already mentioned in the Characterization of regenerated cellulose Section 3.1.1. The use of propyl gallate could reduce the number of chain scission at 110 °C occurring during the dissolution step by 90% as illustrated in Fig. 3a in the grey area through the shift of the chain scission number at 0 h. The medium cellulose-[emim]OAc shows a stable behavior at 60 °C whereas degradation is observed at 90 and 110 °C. A level-off in the number of chain scission can be observed after 5 h of storage time, both at 90 °C and 110 °C. Fig. 3b illustrates the number of chain scission per cellulose chain unit over time calculated using the DP_v of precipitated cellulose after dissolution as DP_0. The degradation taking place prior to storage at elevated temperature is thus excluded. Table 3 summarizes the reaction rate and the levelling-off degree of polymerization of cellulose calculated from models 1 and 2. Both models yielded similar results. The stabilized solution shows a higher rate of cellulose chain scission upon storage than the non-stabilized solution. The obtained higher LODP is thus explained by a significant decrease in cellulose depolymerization during the dissolution step. PG seems to have no stabilizing effect during further storage at elevated temperature.

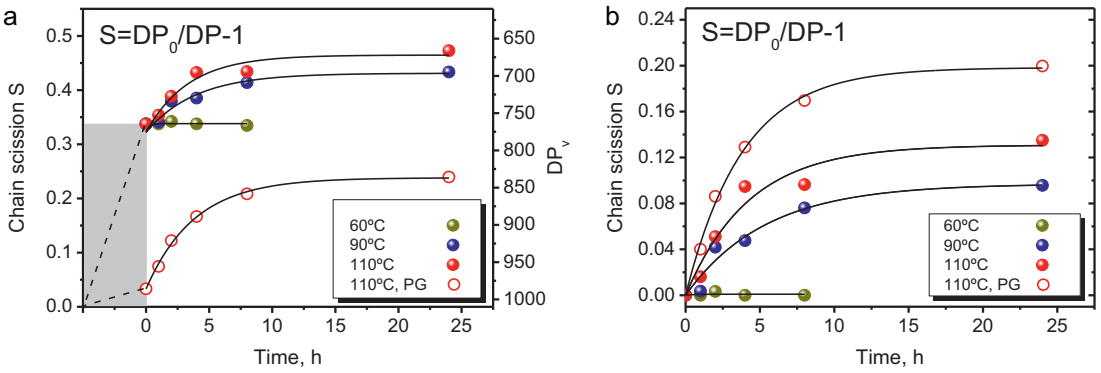

Fig. 3. Scission per cellulose chain versus reaction time using model 2 (Eq. (4)). (a) DP_0 corresponds to the DP_v of the original pulp. (b) DP_0 corresponds to the DP_v of the precipitated cellulose after dissolution.

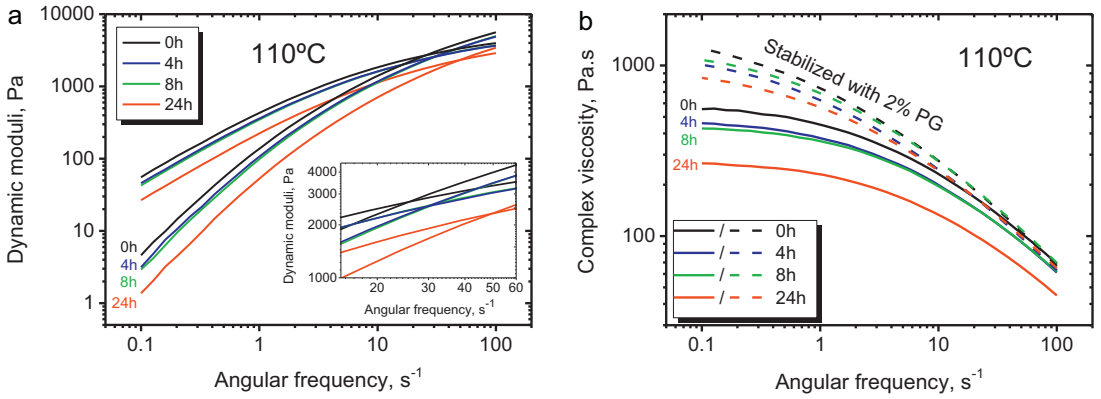

Fig. 4. (a) Dynamic moduli for the stabilized and non-stabilized solutions stored at 110 °C (measured at 60 °C).The inset shows a zoom on the cross-over points. (b) Complex viscosity for the stabilized (dashed line) and non-stabilized (solid line) solutions stored at 110 °C (measured at 60 °C).

3.2. Rheological characterization of cellulose-[emim]OAc

3.2.1. Shear rheological measurements

Fig. 4 depicts the dynamic sweep tests of the cellulose–IL solutions stored at 110 °C. All the oscillatory experiments were conducted at 60 °C. Cellulose–IL solutions exhibit a non-Newtonian viscous behavior which is typical for polymer solutions. Complex viscosity curves show a Newtonian plateau at low angular frequencies followed by a shear thinning behavior at higher frequencies occurring due to the deformation of the cellulose chains that is imposed by the external stresses applied. The dynamic moduli, represented by the loss modulus G'' and the storage modulus G', are referring to the viscous and elastic properties of cellulose–IL solution, respectively. The cross-over point provides information on the visco-elastic behavior of a polymer solution under frequency sweep. At low frequencies, the deformation imposed on the cellulose chains takes place slowly so that the entanglement points of the different polymer chains slip from each other. By increasing the frequency, these entanglements become points of a fixed network and thus the storage modulus increases more rapidly than does the loss modulus until the two curves cross each other. Viscous properties are predominant as long as the loss modulus is larger than the storage modulus (Chen, Zhang, Cheng, & Wang, 2009).

The dynamic frequency sweep of the solutions stored at 60 °C demonstrates the superposition of the reference curve (0 h of storage) and of the curves representing the solutions stored over time which reflects the stability of the cellulose-[emim]OAc system upon time at 60 °C (see Fig. S1 in the Supplemental information). Similar zero-shear viscosities and cross-over moduli and frequencies are thus observed and summarized in Table 4. Rheological values for 90 and 110 °C are also shown in Table 4. Fig. 4 illustrates the response of the cellulose–IL solution stored at 110 °C under shear stresses. The shift of the cross-over point to higher frequency values and the drop of the complex viscosity to lower values represented in Fig. 4a and b, respectively, confirm cellulose depolymerization upon time. The reduction of the cellulose DP_v results in a decrease of cellulose network density which favors a liquid-like behavior of the solution. The cross over point is thus shifted to higher frequencies. Furthermore, the reduction of the number of entanglement points causes a drop of the moduli to lower values.

Table 3
Reaction rate of cellulose degradation and LODP of cellulose in [emim]OAc calculated from models 1 and 2.

	90 °C		110 °C		110 °C, stabilized with 2% PG	
	Mod. 1	Mod. 2	Mod. 1	Mod. 2	Mod. 1	Mod. 2
DP_0 (0 h[a])	767	767	767	767	993	993
k (h^{-1})	0.19	0.18	0.23	0.23	0.26	0.26
LODP	699	699	678	678	828	828

[a] DP of precipitated cellulose after dissolution.

Table 4
Rheological data of cellulose-[emim]OAc dopes.

Original pulp	DP_v	η_0^* (Pa.s)						Cross over point $G' = G''$ (Pa)				ω (s^{-1})			
	1026	–				–				–					
Degradation temperature	110 °C	110 °C				110 °C				110 °C					
	60 °C	90 °C	–	PG	60 °C	90 °C	–	PG	60 °C	90 °C	–	PG	60 °C	90 °C	–	PG	
Storage time	0 h[a]		767[c]		993[c]		601.1		992.9		2703.0		1698.9		25.6		7.5
	1 h[b]	775	764	755	955	590.8	556.9	537.5	954.8	2628.4	2648.0	2409.2	1628.5	25.4	26.3	24.9	7.5
	2 h	764	736	730	914	586.3	536.0	552.2	914.3	2642.4	2595.2	2689.7	1816.7	23.5	27.8	28.2	8.0
	4 h	788	732	701	879	589.9	556.5	489.2	879.5	2681.7	2669.9	2550.1	1673.5	26.4	25.9	29.7	9.3
	8 h	769	713	700	849	575.1	469.8	456.0	849.0	2555.7	2716.2	2635.8	1862.7	25.2	31.8	31.8	9.2
	24 h	–	700	676	828	–	416.1	281.2	827.7	–	2715.1	2321.6	1859.4	–	37.8	49.6	11.8

[a] Characterization of cellulose–IL solution after dissolution.
[b] Characterization of cellulose–IL solution after a storage time of 1 h in the oven.
[c] DP_v of precipitated cellulose after the dissolution step.

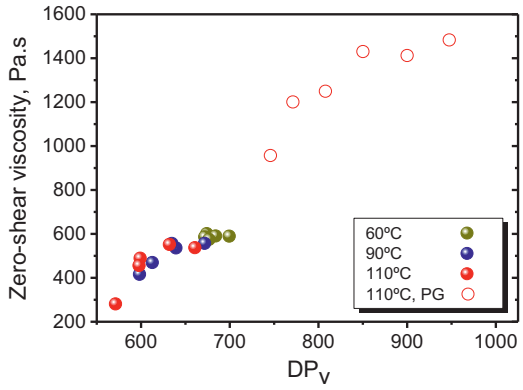

Fig. 5. Zero-shear viscosity versus DP_v for all the solutions.

Fig. 4b shows the complex viscosity curves of the stabilized cellulose samples. The stabilizing effect of PG during the dissolution in [emim]OAc can be observed by the shift of the complex viscosity of the cellulose–IL solution after dissolution (0 h of storage) to higher values. Fig. 5 represents the zero-shear viscosity of the different solutions, calculated by fitting the complex viscosity curves with the three-parameter Cross viscosity model, as a function of the DP_v. It can be clearly seen that the zero-shear viscosity, which describes the viscosity at infinitesimal shear or at rest, is directly linked to the extension of the polymer entanglement network. Higher cellulose DP_v or molecular weight increases the polymer network and thus the zero-shear viscosity. Dynamic measurements offer the possibility to monitor the degradation of cellulose in ILs by the reduction of the complex viscosity and the shift of the cross over point of the dynamic moduli to higher frequencies.

3.2.2. *Extensional rheological measurements*

When cellulose solutions are processed to form fibers and films, the polymers in solution are not only subjected to shear stress but also undergo elongational deformation. In particular during dry-jet wet spinning the liquid filaments pass an air gap in which they are drawn to increase the total cellulose orientation via a uniaxial extensional stress. This lyocell process has been demonstrated to be suitable for spinning of high-performance cellulosic fibers from ionic liquid solutions (Fink et al., 2001; Hummel et al., 2014). It is thus of interest to monitor the effects of cellulose depolymerization on the elongational-viscoelastic properties of the solution to assure good spinnability and spin stability. The capillary break-up extensional rheometer (CaBER) allows for the measurement of the apparent transient elongational viscosity and – under certain prerequisites – extensional relaxation time. The latter can be extracted from the measurement data if the elasto-capillary region during the break-up experiment can be identified unambiguously. Fig. 6 shows the diameter evolution versus time of the unstabilized cellulose-[emim]OAc samples stored at 110 °C.

As described in Section 2.2.3, a CaBER experiment can be divided into 4 regions where different factors govern the viscoelastic thinning process. In regime I, the filament thinning profile is ill-defined due to gravitational effects overlapping the capillary forces. Using a local bond number of 0.2, a threshold filament diameter of 1.60 mm upon which gravitation contributes only insignificantly to the filament thinning profile could be calculated. In regime II, the capillary driven flow is resisted by the dominating viscous stress, resulting in a linear decay of the filament diameter (Anna & McKinley, 2001; Clasen, 2010; Haward et al., 2012). The subsequent regime III represents a transition phase where visco-capillary balance as observed in regime II is superimposed by an incipient extensional thinning, originating from a pronounced disentanglement and orientation of the cellulose chains. Ultimately, the filament thinning is governed

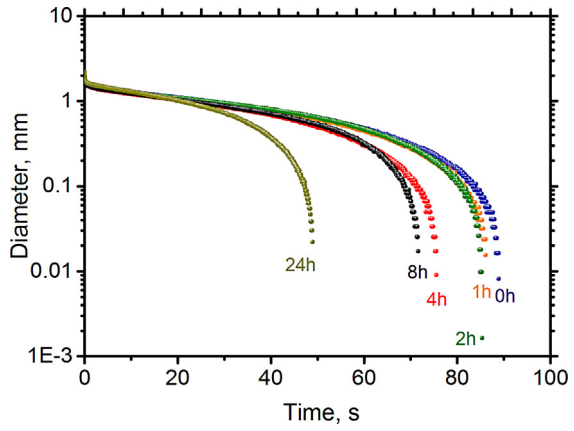

Fig. 6. Evolution of the mid-filament diameter vs. time for cellulose-[emim]OAc solutions stored at 110 °C.

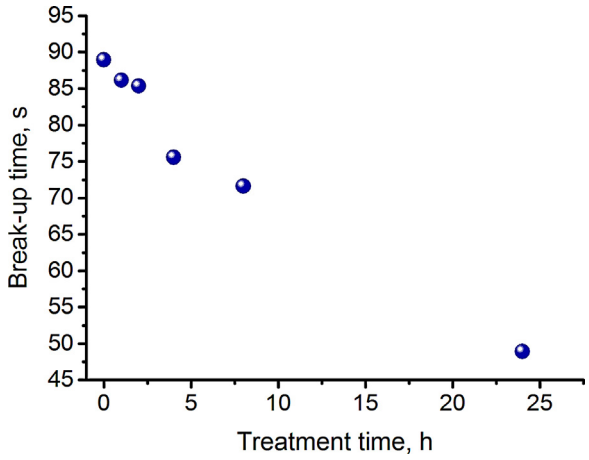

Fig. 8. CaBER break-up time of unstabilized samples stored at 110 °C.

by a balance of the surface pressure and the elastic stress of the unraveling polymer chains. This regime IV is observed only at very high strains and thus at a late stage of the measurement close to filament break-up. Clasen (2010) has demonstrated that regime IV can be identified when plotting the extension rate and apparent extensional viscosity versus time (Fig. 7a). Regime IV is characterized by a small but distinct rise of the apparent extensional viscosity close to the final break-up (strain-hardening). Concomitantly, the extensional rate should reach a plateau value after rising with time. As illustrated in Fig. 7a, neither the rise of the apparent extensional viscosity nor the plateau of the extension rate as described by Clasen (2010) can be observed.

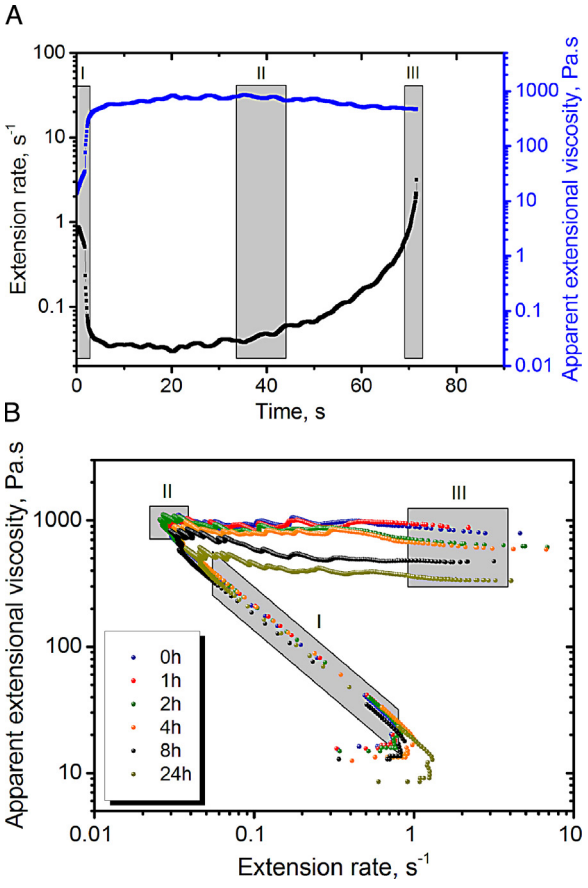

Fig. 7. (a) Extension rate and apparent extensional viscosity versus time for the unstabilized cellulose-[emim]OAc solutions stored for 8 h at 110 °C. (b) Apparent extensional viscosity as a function of the extension rate for the unstabilized cellulose-[emim]OAc solutions stored for 8 h at 110 °C.

Fig. 7b shows the apparent extensional viscosity as a function of the extension rate. Elasto-capillary response would cause a steep rise of η_E which is clearly not observed in our case. Thus, a concentration of 10 wt% is too high and the CaBER measurement is not sensitive enough to detect the elasto-capillary region. This means that extensional relaxation times cannot be extracted from the CaBER experiments.

However, a clear correlation between the storage time of the solution and the filament break-up time was found. Fig. 8 shows the break-up time of unstabilized samples stored at 110 °C. Using the same CaBER settings throughout all measurements, the time for final filament rupture is clearly reduced upon prolonged storage at 110 °C. The advancing depolymerization of the cellulose results in shorted chains which exert a reduced visco-elastic stress counteracting the capillary pressure. Thus the filament is thinning faster and breaking sooner. This is an important finding for cellulose solution spinning. As mentioned, the key-feature of dry-jet wet spinning of polymer solutions is the possibility to draw the filament in the air-gap. This, however, requires the necessary elongational properties and stability of the liquid filament. Uncontrolled cellulose depolymerization reduces this stability, leads to filament breaks in the air gap, and, ultimately, deteriorates the spinnability.

4. Conclusion

A study on the thermal stability of cellulose in [emim]OAc upon storage was conducted using traditional and rheological methods. The determination of the intrinsic viscosity and the molar mass distribution of the coagulated cellulose established that cellulose depolymerization mainly occurs during the first hours of storage at temperatures over 90 °C. Degradation of cellulose chains in IL was also monitored by investigating the behavior of the cellulose-[emim]OAc solutions under shear and extensional stresses by using dynamic shear rheology and capillary break-up extensional rheology, respectively. The drop of the complex viscosity to lower values and the shift of the cross over point of the storage and loss moduli to higher frequency values demonstrate a liquid-like behavior of the solution after long storage at high temperature as a direct result of the reduction of the cellulose DP. The liquid-like behavior of the cellulose-[emim]OAc solutions stored at high temperature is confirmed by the faster thinning and shorter breakup times obtained during extensional measurements. It was thus shown that shear and elongational rheology are two methods that can be used to monitor cellulose depolymerization in IL. Shear and

elongational visco-elastic properties of cellulose-[emim]OAc solution are the key-feature of a successful dry-jet wet spinning. The uncontrolled depolymerization of cellulose occurring in [emim]OAc at high temperature reduces the spinnability due to its impact on the rheological properties of the polymer solution. In addition, mono and oligomeric degradation products may accumulate in the spent ionic liquid which necessitates appropriate recycling strategies. These results will promote the understanding and the establishment of a stable dry-jet wet spinning of cellulose–ionic liquid solution for the production of fibers and films.

Acknowledgements

This study is part of the Future Biorefinery project founded by the Finnish Bioeconomy Cluster and TEKES (Finnish Founding Agency for Technology and Innovation).

Appendix A. Supplementary data

Supplementary data associated with this article can be found, in the online version, at http://dx.doi.org/10.1016/j.carbpol.2014.09.075.

References

Anna, S. L., & McKinley, G. H. (2001). Elasto-capillary thinning and breakup of model elastic liquids. *Journal of Rheology (1978–Present)*, *45*(1), 115–138.
Berggren, R., Berthold, F., Sjöholm, E., & Lindström, M. (2003). Improved methods for evaluating the molar mass distributions of cellulose in kraft pulp. *Journal of Applied Polymer Science*, *88*(5), 1170–1179.
Borrega, M., Tolonen, L. K., Bardot, F., Testova, L., & Sixta, H. (2013). Potential of hot water extraction of birch wood to produce high-purity dissolving pulp after alkaline pulping. *Bioresource Technology*, *135*, 665–671.
Calvini, P. (2005). The influence of levelling-off degree of polymerisation on the kinetics of cellulose degradation. *Cellulose*, *12*(4), 445–447.
Calvini, P., & Gorassini, A. (2006). On the rate of paper degradation: Lessons from the past. *Restaurator*, *27*(4), 275–290.
Calvini, P., Gorassini, A., & Merlani, A. L. (2008). On the kinetics of cellulose degradation: Looking beyond the pseudo zero order rate equation. *Cellulose*, *15*(2), 193–203.
Cao, Y., Wu, J., Zhang, J., Li, H., Zhang, Y., & He, J. (2009). Room temperature ionic liquids (RTILs): A new and versatile platform for cellulose processing and derivatization. *Chemical Engineering Journal*, *147*(1), 13–21.
Chen, X., Zhang, Y., Cheng, L., & Wang, H. (2009). Rheology of concentrated cellulose solutions in 1-butyl-3-methylimidazolium chloride. *Journal of Polymers and the Environment*, *17*(4), 273–279.
Clasen, C. (2010). Capillary breakup extensional rheometry of semi-dilute polymer solutions. *Korea-Australia Rheology Journal*, *22*(4), 331–338.
Collier, J., Watson, J., Collier, B., & Petrovan, S. (2009). Rheology of 1-butyl-3-methylimidazolium chloride cellulose solutions. II. Solution character and preparation. *Journal of Applied Polymer Science*, *111*(2), 1019–1027.
Ding, H., & Wang, Z. (2008). On the degradation evolution equations of cellulose. *Cellulose*, *15*(2), 205–224.
Dupont, A., & Mortha, G. (2004). Comparative evaluation of size-exclusion chromatography and viscometry for the characterisation of cellulose. *Journal of Chromatography A*, *1026*(1), 129–141.
Eichinger, D. (2012). A vision of the world of cellulosic fibers in 2020. *Lenzinger Berichte*, *90*, 1–7.
Feng, L., & Chen, Z. (2008). Research progress on dissolution and functional modification of cellulose in ionic liquids. *Journal of Molecular Liquids*, *142*(1), 1–5.
Fink, H. P., Weigel, P., Purz, H., & Ganster, J. (2001). Structure formation of regenerated cellulose materials from NMMO-solutions. *Progress in Polymer Science*, *26*(9), 1473–1524.
Gericke, M., Schlufter, K., Liebert, T., Heinze, T., & Budtova, T. (2009). Rheological properties of cellulose/ionic liquid solutions: From dilute to concentrated states. *Biomacromolecules*, *10*(5), 1188–1194.
Hauru, L. K., Ma, Y., Hummel, M., Alekhina, M., King, A. W., Kilpeläinen, I., et al. (2013). Enhancement of ionic liquid-aided fractionation of birchwood. Part 1: Autohydrolysis pretreatment. *RSC Advances*, *3*(37), 16365–16373.
Haward, S. J., Sharma, V., Butts, C. P., McKinley, G. H., & Rahatekar, S. S. (2012). Shear and extensional rheology of cellulose/ionic liquid solutions. *Biomacromolecules*, *13*(5), 1688.
Hermanutz, F., Gähr, F., Uerdingen, E., Meister, F., & Kosan, B. (2008). New developments in dissolving and processing of cellulose in ionic liquids? *Macromolecular Symposia*, *262*(1), 23–27.
Hummel, M., Michud, A., Tanttu, M., Asaadi, S., Ma, Y., Hauru, L. K. J., et al. (2014). Ionic liquids for the production of man-made cellulosic fibers-opportunities and challenges. *Advances in Polymer Science*, accepted
Kosan, B., Michels, C., & Meister, F. (2008). Dissolution and forming of cellulose with ionic liquids. *Cellulose*, *15*(1), 59–66.
Liebert, T., & Heinze, T. (2008). Interaction of ionic liquids with polysaccharides 5. Solvents and reaction media for the modification of cellulose. *BioResources*, *3*(2), 576–601.
Lu, F., Cheng, B., Song, J., & Liang, Y. (2012). Rheological characterization of concentrated cellulose solutions in 1-allyl-3-methylimidazolium chloride. *Journal of Applied Polymer Science*, *124*(4), 3419–3425.
Perepelkin, K. (2007). Lyocell fibres based on direct dissolution of cellulose in *N*-methylmorpholine *N*-oxide: Development and prospects. *Fibre Chemistry*, *39*(2), 163–172.
Pinkert, A., Marsh, K. N., Pang, S., & Staiger, M. P. (2010). Ionic liquids and their interaction with cellulose. *ChemInform*, *41*(17), no–no.
Roselli, A., Hummel, M., Monshizadeh, A., Maloney, T., & Sixta, H. (2014). Ionic liquid extraction method for upgrading eucalyptus kraft pulp to high purity dissolving pulp. *Cellulose*, *21*, 3655–3666.
Rosenau, T., Potthast, A., Adorjan, I., Hofinger, A., Sixta, H., Firgo, H., & Kosma, P. (2002). Cellulose solutions in *N*-methylmorpholine-*N*-oxide (NMMO)—Degradation processes and stabilizers. *Cellulose*, *9*(3), 283–291.
Sammons, R. J., Collier, J. R., Rials, T. G., & Petrovan, S. (2008a). Rheology of 1-butyl-3-methylimidazolium chloride cellulose solutions. III. Elongational rheology. *Journal of Applied Polymer Science*, *110*(5), 3203–3208.
Sammons, R. J., Collier, J. R., Rials, T. G., & Petrovan, S. (2008b). Rheology of 1-butyl-3-methylimidazolium chloride cellulose solutions. I. Shear rheology. *Journal of Applied Polymer Science*, *110*(2), 1175–1181.
Simmons, T. J., Lee, S. H., Miao, J., Miyauchi, M., Park, T., Bale, S. S., et al. (2011). Preparation of synthetic wood composites using ionic liquids. *Wood Science and Technology*, *45*(4), 719–733.
Stefanescu, C., Daly, W. H., & Negulescu, I. I. (2012). Biocomposite films prepared from ionic liquid solutions of chitosan and cellulose. *Carbohydrate Polymers*, *87*(1), 435–443.
Stelter, M., Brenn, G., Yarin, A., Singh, R., & Durst, F. (2000). Validation and application of a novel elongational device for polymer solutions. *Journal of Rheology (1978–Present)*, *44*(3), 595–616.
Stelter, M., Brenn, G., Yarin, A., Singh, R., & Durst, F. (2002). Investigation of the elongational behavior of polymer solutions by means of an elongational rheometer. *Journal of Rheology (1978–Present)*, *46*(2), 507–527.
Swatloski, R. P., Spear, S. K., Holbrey, J. D., & Rogers, R. D. (2002). Dissolution of cellulose with ionic liquids. *Journal of the American Chemical Society*, *124*(18), 4974–4975.
The Fiber Year. (2013). *World survey on textiles & nonwovens 2013*. The Fiber Year.
Wendler, F., Kosan, B., Krieg, M., & Meister, F. (2009). Possibilities for the physical modification of cellulose shapes using ionic liquids? *Macromolecular Symposia*, *280*(1), 112–122.
Wendler, F., Todi, L. N., & Meister, F. (2012). Thermostability of imidazolium ionic liquids as direct solvents for cellulose. *Thermochimica Acta*, *528*, 76–84.
Wu, R., Wang, X., Li, F., Li, H., Wang, Y., & Green composite films prepared from cellulose, starch and lignin in room-temperature ionic liquid. (2009). *Bioresource Technology*, *100*(9), 2569–2574.